

¹ Drought indices of water demand and supply and their impact on LULCC
² in Chile from ERA5-Land and MODIS

³ Francisco Zambrano^{a,1,*}

^a Universidad Mayor, Hémera Centro de Observación de la Tierra, Facultad de Ciencias, Escuela de Ingeniería en Medio Ambiente y Sustentabilidad, Santiago, Chile, 7500994

⁴ **Abstract**

Central Chile has been the focus of research studies due to the persistent decrease in water supply, which is impacting the hydrological system and vegetation development. This persistent period of water scarcity has been defined as a “Mega Drought”. Our objective is to examine the effects of drought on LULCC (land use land cover change) over continental Chile using drought indices of water supply and demand, soil moisture, and vegetation productivity. For the analysis, continental Chile was divided into five zones according to a latitudinal gradient: “Norte Grande,” “Norte Chico,” “Centro,” “Sur,” and “Austral.” The monthly ERA5-Land (ERA5L) variables for precipitation, temperature, and soil moisture were used. From 2001 to 2022, we used the land cover MODIS product MCD12Q1, and from 2000 to 2023, we used the NDVI (Normalized Difference Vegetation Index) product MOD13A3 collection 6.1. We estimated atmospheric evaporative demand (AED) using the Hargreaves-Samani equation with the ERA5L temperature. We used the Standardized Precipitation Index (SPI), the Standardized Precipitation Evapotranspiration Index (SPEI), the Evaporative Demand Drought Index (EDDI), the Standardized Soil Moisture Index (SSI), and the Standardized anomaly of cumulative NDVI (zcNDVI) as drought indicators. These indices were calculated for time scales of 1, 3, 6, 12, 24, and 36 months, except for zcNDVI, which was for 6 months. We analyze the trend for LULCC, vegetation productivity, and drought indices. Also, we analyzed the temporal correlation of SPI, SPEI, EDDI, and SSI with zcNDVI to gain insights into the impact of water supply and demand on vegetation productivity. Our results showed that LULCC were highest in “Centro,” “Sur,” and “Austral,” with 36%, 31%, and 34%, respectively. The EDDI shows that water demand has increased for all zones, with a major increase in “Norte Grande.” The drought indices of water supply and soil moisture evidence a decreasing trend, which decreases at longer time scales, from “Norte Grande” to “Sur.” “Austral” is the only zone that shows an increase in supply. Vegetation productivity measures by zcNDVI present a negative trend in “Norte Chico” and “Centro.” Showing to be the zones most impacted by climatic conditions, the years 2020 and 2022 suffered the most extreme drought. On the other hand, forests seem to be the most resistant to drought. The types that show to be most affected by variation in climate conditions are shrublands, savannas, and croplands. The drought indices that have the capability of explaining to a major degree the variance in vegetation productivity are SSI-12, followed by SPEI-24 and SPEI-12 in “Norte Chico” and “Centro.” The results indicate that “Norte Chico” and “Zona Central” are the most sensitive regions to water supply deficits longer than a year, potentially explained by a low capacity of water storage in those zones that should be further investigated.

⁵ **Keywords:** drought, land cover change, satellite

*Corresponding author

Email address: francisco.zambrano@umayor.cl (Francisco Zambrano)

¹This is the first author footnote.

6 **1. Introduction**

7 The sixth assessment report (AR6) of the IPCC [1] indicates that human-induced greenhouse gas emissions
8 have increased the frequency and/or intensity of some weather and climate extremes, and the evidence has
9 been strengthened since AR5 [2]. There is a high degree of confidence that rising temperatures will increase
10 the land area where droughts will occur more frequently and with greater severity [3]. Furthermore, drought
11 increases tree mortality and triggers changes in land cover and, consequently, land use, thus impacting
12 ecosystems [4]. Nevertheless, there is a lack of understanding of how the alteration in water supply and
13 demand is affecting land cover transformations.

14 The primary cause of drought is precipitation, and temperature makes it worse [5]. Drought impacts soil
15 moisture, hydrological regimes, and vegetation productivity. Initially, drought was commonly classified as
16 meteorological, hydrological, and agricultural [6]. Lately, [7] and [8] have given an updated definition of
17 drought for the Anthropocene, suggesting that it should be considered the feedback of humans' decisions
18 and activities that drives the anthropogenic drought. Even though it has been argued that those definitions
19 do not fully address the ecological dimensions of drought, [4] proposed the ecological drought definition as
20 "an episodic deficit in water availability that drives ecosystems beyond thresholds of vulnerability, impacts
21 ecosystem services, and triggers feedback in natural and/or human systems.". Moreover, many ecological
22 studies have misinterpreted how to characterize drought, for example, sometimes considering "dry" con-
23 ditions as "drought" [9]. On the other hand, the AR6 [1] predicts that many regions of the world will
24 experience more severe agricultural and ecological droughts even if global warming stabilizes at 1.5°–2°C.
25 Then, there is a challenge in conducting drought research, especially to evaluate its impact on ecosystems.

26 Chile has been facing a persistent rainfall deficit for more than a decade [10], which has impacted vegeta-
27 tion development [11] and the hydrological system [12]. Current drought conditions have affected crop
28 productivity [13, 14], forest development [15, 16], forest fire occurrence [17], land cover change [18], water
29 supply in watersheds [19], and have had economic impacts [20]. In 2019–2020, the drought severity reached
30 an extreme condition in Central Chile (30–34°S) not seen for at least 40 years, and the evidence indicates
31 that the impact is transversal to the land cover classes of forest, grassland, and cropland [11]. The prolonged
32 lack of precipitation in Central Chile is producing changes in ecosystem dynamics that must be studied.

33 For the spatiotemporal assessment of drought impact (i.e., by water supply and demand) on land cover
34 changes, we need climatic reliable variables such as precipitation, temperature, soil moisture, land cover, and
35 vegetation status. For developing countries like Chile, the weather networks present several disadvantages,
36 such as gaps, a short history, and low-quality data. Reanalysis data, as the ERA5-Land (ERA5L) [21]
37 provides hourly climatic information (precipitation, temperature, and soil moisture) without gaps since
38 1950 with global extension. ERA5L has already been used for drought assessment using the Standardized
39 Precipitation-Evapotranspiration Index (SPEI) [22] and for flash drought [23] by analyzing soil moisture and
40 evapotranspiration. On the other hand, satellite remote sensing [24, 25] is the primary method to evaluate
41 how drought impacts vegetation dynamics. The Moderate-Resolution Imaging Spectroradiometer (MODIS)
42 can be used to get vegetation drought indices (VDI), which are often used as proxies for productivity
43 [26, 27]. Besides, land use and land cover (LULC) change can be driven by drought [28, 29]. To analyze
44 these changes, multiple LULC products exist [30]. One of those that provides time series since 2001 is the
45 MCD12Q1 [31] from MODIS. The variation in water supply and demand is finally reflected in the total
46 water storage (TWS). The Gravity Recovery and Climate Experiment (GRACE), which allows analyzing
47 changes in water availability at coarse resolution, can retrieve the TWS [32, 33]. We can find drought
48 indices of supply (i.e., precipitation) and demand (i.e., temperature) using climatic reanalysis (ERA5L) and
49 vegetation data (MODIS). This lets us figure out how drought changes LULC. Further, the TWS can be
50 assessed with regard to the changes in water supply and demand to gain insight into the impact on water
51 storage.

52 To evaluate meteorological drought (i.e., water supply), the World Meteorological Organization (WMO;
53 [34]) recommends the Standardized Precipitation Index (SPI; [35]), a multiscalar drought index that allows
54 to monitor precipitation deficits from short- to long-term. Following the same approach, [36] incorporates

55 into the SPI the effect of temperature through the use of potential evapotranspiration, thus proposing the
56 SPEI (Standardized Precipitation Evapotranspiration Index). Similarly, to evaluate solely the evaporative
57 demand driven by temperature, [37] and [38] came up with the Evaporative Demand Drought Index (EDDI).
58 For vegetation, in a similar manner as the SPI, SPEI and EDDI; [14] proposed the zcNDVI, a standardized
59 anomaly of the cumulative Normalized Difference Vegetation Index (NDVI), which could be accumulated
60 over the growing season or any period (e.g., months), resulting in a multiscale drought index. For soil
61 moisture, several drought indices exist, such as the Soil Moisture Deficit Index (SDMI) a normalized index
62 [39] and the Soil Moisture Agricultural Drought Index (SMADI) [40] which is a normalized index using
63 vegetation, land surface temperature, and a vegetation condition index (VCI, [41]). From TWS, we can
64 estimate the standardized terrestrial water storage index (STI) [42], a standardized anomaly that follows
65 the methodology of the SPI, SPEI, EDDI, and zcNDVI. Thereby, we have drought indices for water supply,
66 demand, and storage, which can help to make a comprehensive assessment of drought.

67 In this research, we aim to analyze the impact of drought on different types of ecosystems (land cover
68 classes) in continental Chile. Our specific goals are: i) to analyze the trend on multi-scalar drought indices
69 for water demand and supply, soil moisture, and vegetation productivity for 1981–2023/2001–2023; ii) to
70 assess the LULC change for 2001–2022 and how it relates to drought indices; iii) to evaluate the relationship
71 between zcNDVI, a measure of vegetation productivity, and drought indices for water demand and supply
72 and soil moisture; and iv) to assess if the observed changes in the drought indices are linked to TWS.

73 2. Study area

74 Continetal Chile has a diverse climate condition from north to south and east to west [43] (Figure 1), which
75 determines its great ecosystem diversity (Figure 2). The Andes Mountains are a main factor in latitudinal
76 variation [44]. To describe the climate and ecosystem of Chile, we use the Koppen-Geiger release by [45] and
77 the land cover type persistance of 80% of times for 2001–2022, from the IGBP classification scheme [31] (see
78 Section 3.4). “Norte Grande” and “Norte Chico” predominate in an arid desert climate with hot (Bwh) and
79 cold (Bwk) temperatures. At the south of “Norte Chico,” the climate changes to an arid steppe with cold
80 temperatures (Bsk). Mainly, the land is barren, with a minor surface of vegetation types such as shrubland
81 and grassland. In the zones “Centro” and the north half of “Sur,” the main climate is Mediterranean, with
82 warmer to hot summers (Csa and Csb). There is a significant amount (50%) of Chilean matorral (shrubland
83 and savanna, [18]), then grassland (16%), forest (8%), and croplands (5%), in “Centro.” The south part of
84 “Sur” and the north part of “Austral” are dominated by an oceanic climate (Cfb). Those zones are high in
85 forest and grassland. The southern part of the country has a tundra climate, and in Patagonia, it is a cold
86 semi-arid area with an extended surface of grassland, forest, and, to a lesser extent, savanna.

87 3. Materials and Methods

88 3.1. Software and packages used

89 For the downloading, processing, and analysis of the spatio-temporal data, we used the open source software
90 for statistical computing and graphics, R [46]. For downloading ERA5L, we used the `{ecmwfr}` package [47].
91 For processing raster data, we used `{terra}` [48] and `{stars}` [49]. For managing vectorial data, we used
92 `{sf}` [50]. For the calculation of AED, we used `{SPEI}` [51].

93 3.2. Data

94 3.2.1. Earth observation data

95 For water supply and demand variables, we used ERA5L [21], a reanalysis dataset that provides the evolution
96 of land variables since 1950. It has a spatial resolution of 0.1° , hourly frequency, and global coverage. We

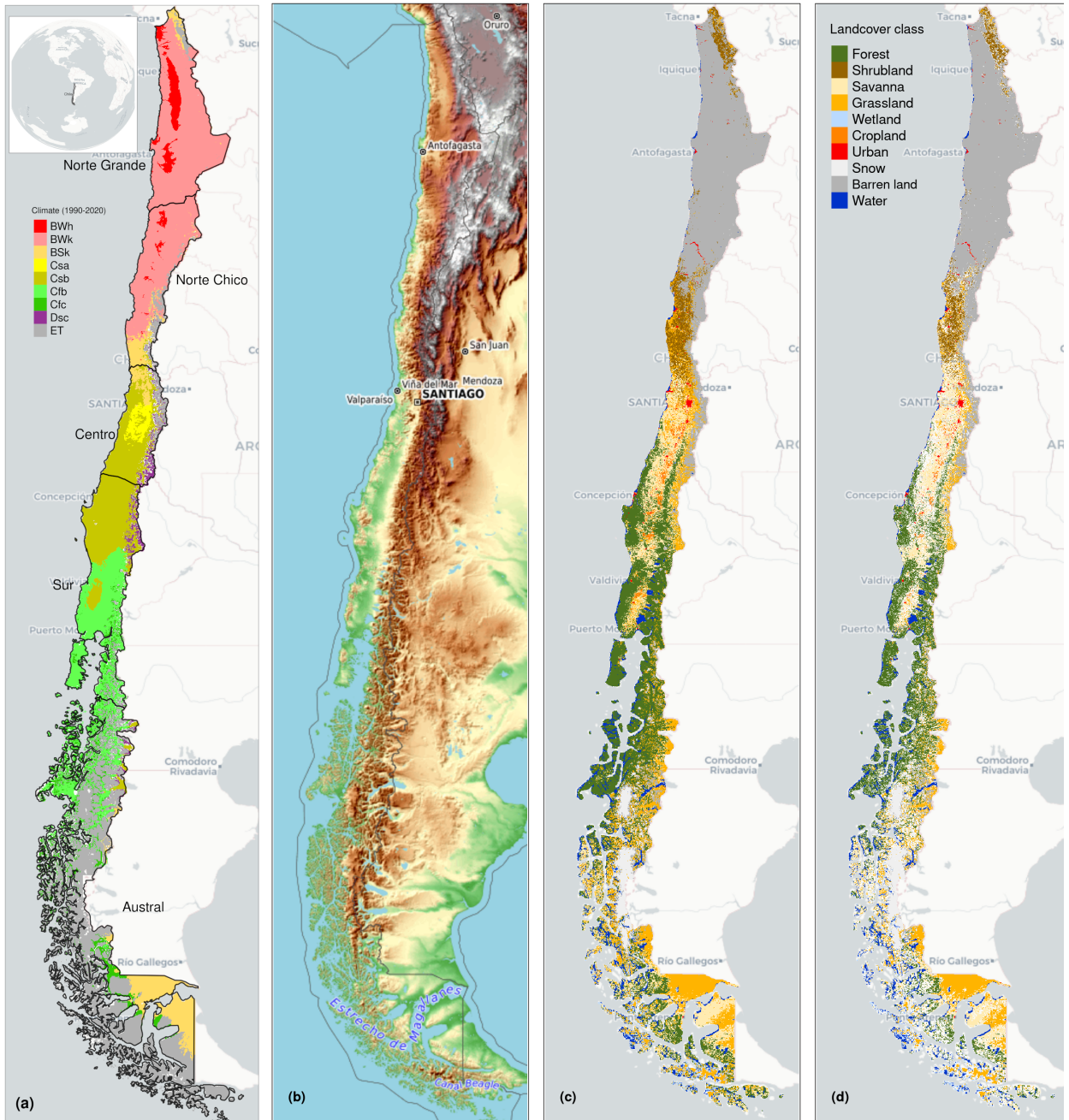


Figure 1: (a) Chile with the Koppen-Geiger climate classes and the five macrozones “Norte Grande”, “Norte Chico”, “Centro”, “Sur”, and “Austral”. (b) Topography reference map. (c) Land cover classes for 2022. (d) Persistent land cover classes (> 80%) for 2001-2022

97 selected the variables for total precipitation, 2 meter temperature maximum and minimum, and volumetric
 98 soil water layers between 0 and 100cm of depth (layer 1 to layer 3). The data was downloaded using the
 99 Copernicus Climate Data Store (CDS) Application Program Interface (API) implemented in `{ecmfwr}` [47].

100 To derive a proxy of vegetation productivity, we used the product MOD13A3 collection 6.1 from MODIS
 101 [52]. It provides vegetation indices (NDVI and EVI) at 1km of spatial resolution and monthly frequency. The

¹⁰² MOD13A3.061 and MCD12Q1.061 were retrieved from the online Data Pool, courtesy of the NASA EOSDIS
¹⁰³ Land Processes Distributed Active Archive Center (LP DAAC), USGS Earth Resources Observation and
¹⁰⁴ Science (EROS) Center, Sioux Falls, South Dakota, <https://lpdaac.usgs.gov/tools/data-pool/>.

Table 1: Description of the earth observation data used

Product	Sub-product	Variable	Spatial Resolution	Period	Units	Short Name
ERA5L		Precipitation	0.1°	1981-2023	mm	P
		Maximum temperature			°C	T_{max}
		Minimum temperature			°C	T_{min}
		Volumetric Soil Water Content at 1m			m3/m3	SM
ERA5L*	MOD13A3.061	Atmospheric Evaporative Demand	0.1°	1981-2023	mm	AED
MODIS		Normalized Difference Vegetation Index	1 km	2000-2023		NDVI
		land cover IGBP scheme		2001-2022		land cover

*Derived from ERA5L with Eq. 1.

¹⁰⁵ 3.2.2. Weather stations

¹⁰⁶ We compared the ERA5L variables for monthly mean temperature, total precipitation, and volumetric soil
¹⁰⁷ water content against values retrieved by weather stations. For temperature and precipitation, we used the
¹⁰⁸ weather network from the Ministry of Agriculture of Chile (www.agromet.com) between 2015 and 2023. We
¹⁰⁹ used 277 stations located throughout Chile. For soil moisture, we select a private soil network that is owned
¹¹⁰ by the agricultural enterprise Garcés Fruit, which has 99 stations in Central Chile, located in cherry fruit
¹¹¹ crops. We used daily data for the year 2022 and the months outside the growing season, May to September,
¹¹² to avoid the effect of irrigation on soil moisture, which is hardly captured by ERA5L.

¹¹³ 3.2.3. Validation of ERA5L variables

¹¹⁴ To account for the performance of the ERA5L climatic variables regarding the values measured by the
¹¹⁵ weather stations. We selected the following metrics:

$$\text{MAE} = \frac{1}{n} \sum |E - S|$$

$$\text{Bias} = \frac{\sum E}{\sum S}$$

$$\text{ubRMSE} = \sqrt{\frac{\sum [(E_i - \bar{E}) - (S_i - \bar{S})]^2}{n}}$$

$$CC = \frac{\sum (S_i - \bar{S})(E_i - \bar{E})}{\sqrt{(S_i - \bar{S})^2(E_i - \bar{E})^2}}$$

¹¹⁶ MAE: mean absolute error bias: bias ubRMSE: unbiassed root mean squared error CC: coefficient of
¹¹⁷ correlation S: value of the variable measure by the weather station E: value of the variable measure by
¹¹⁸ ERA5L

121 3.3. Drought Indices

122 3.3.1. Atmospheric Evaporative Demand (AED)

123 For the indices EDDI and SPEI that use water demand, first we have to calculate the AED. For this, we
124 used the method of Hargreaves [53, 54]:

$$AED = 0.0023 \cdot Ra \cdot (T + 17.8) \cdot (T_{max} - T_{min})^{0.5} \quad (1)$$

125 where Ra ($MJ\ m^2\ day^{-1}$) is extraterrestrial radiation; T , T_{max} , and T_{min} are mean, maximum, and
126 minimum temperature ($^{\circ}C$). We calculate the centroid coordinates per pixel and use the latitude to estimate
127 Ra .

128 We chose the method of Hargreaves to estimate AED because of its simplicity, which only requires tem-
129 peratures and extrarrestrial radiation. Also, it has been recommended over other methods when the use of
130 several climatic variables is limited [55].

131 3.3.2. Non-parametric calculation of drought indices

132 We derived the drought indices of water supply and demand, soil moisture from the ERA5L dataset, and
133 vegetation from the MODIS product, all at monthly frequency.

134 To evaluate water demand, we chose the *EDDI* [37, 38] index, which uses the *AED*. For supply, we used
135 the index recommended by the World Meteorological Organization (WMO) for monitoring drought, the
136 *SPI* [35]. We calculated the *SPEI*, which used a balance between P and *AED*, in this case, an auxiliary
137 variable $D = P - AED$ is used. In this study, we used the *SSI* (standardized soil moisture index at 1 m)
138 [56, 57], which uses soil moisture at 1m depth. Finally, for the proxy of productivity, *zcNDVI*, we used the
139 *NDVI*. Before using the *NDVI*, it was smoothed using a locally-weighted polynomial regression, following
140 the procedure described in [14] and [13].

141 All the indices are multi-scalar and were calculated for time scales of 1, 3, 6, 12, 24, and 36 months, except
142 for *zcNDVI*, which was calculated for 6 months. The goal is to be able to evaluate short- and long-term
143 droughts in water demand and supply and soil moisture. This is particularly important for central Chile
144 because it has suffered from a prolonged decrease in precipitation for more than 12 years [58, 12, 10].

145 To calculate the drought indices, first we must calculate the accumulation of the variable. In this case, for
146 generalization purposes, we will use V , referring to P , *AED*, D , *NDVI*, and *SM* (Table 1). We cumulated
147 each V over the time series of n values, and for the time scales s :

$$A_{si} = \sum_{i=n-s-i+2}^{n-i+1} V_i \quad \forall i \geq n - s + 1 \quad (2)$$

148 It corresponds to a moving window (convolution) that sums the variable for s starting for the last month
149 n until the month, which could sum for s months ($n-s+1$). Once the variable is cumulated over time for
150 the scale s , we used a nonparametric approach following [37] to derive the drought indices. Thus, the
151 empirically derived probabilities are obtained through an inverse normal approximation [59]. Then, we
152 used the empirical Tukey plotting position [60] over A_i to derive the $P(A_i)$ probabilities across a period of
153 interest:

$$P(A_i) = \frac{i - 0.33}{n + 0.33} \quad (3)$$

154 The drought indices *SPI*, *SPEI*, *EDDI*, *SSI*, and *zcNDVI* are obtained following the inverse normal
155 approximation:

$$DI(A_i) = W - \frac{C_0 + C_1 \cdot W + c_2 \cdot W^2}{1 + d_1 \cdot W + d_2 \cdot W^2 + d_3 \cdot W^3} \quad (4)$$

156 DI is referring to the drought index calculated for the variable V . The values for the constats are:
157 $C_0 = 2.515517$, $C_1 = 0.802853$, $C_2 = 0.010328$, $d_1 = 1.432788$, $d_2 = 0.189269$, and $d3 = 0.001308$. For
158 $P(A_i) \leq 0.5$, $W = \sqrt{-2 \cdot \ln(P(A_i))}$, and for $P(A_i) > 0.5$, replace $P(A_i)$ with $1 - P(A_i)$ and reverse the sign
159 of $DI(A_i)$.

160 *3.4. LULC change for 2001-2022 and its relation with water supply and demand, and soil moisture*

161 *3.4.1. Land cover macroclases and validation*

162 To analyze the LULCC, we use the IGBP scheme from the MCD12Q1 collection 6.1 from MODIS. This
163 product has a yearly frequency from 2001 to 2022. The IGBP defines 17 classes; from these, we regrouped
164 into ten macroclasses, as follows: classes 1-4 to forest, 5-7 to schrublands, 8-9 to savannas, 10 as grasslands,
165 11 as wetlands, 12 and 14 to croplands, 13 as urban, 15 as snow and ice, 16 as barren, and 17 to water
166 bodies. Thus, we have a land cover raster time-series with the ten classes for 2001 and 2023.

167 To validate the land cover obtained, we compare the macroclasses with the ones of a more detailed land
168 cover map made by [61] for Chile with samples acquired in the years 2013–2014 (LCChile). The later has
169 a spatial resolution of 30 m and three levels of defined classes; from those, we used level 1, which fits with
170 the macroclasses land cover. We chose the years 2013 (IGBP2013) and 2014 (IGBP2014) from land cover
171 macrolcasses to validate with LCChile.

172 We follow the next procedure:

- 173 i) resampled LCChile to the spatial resolution (500m) of the land cover macroclasses using the nearest
174 neighbor method,
- 175 ii) took a random sample of 1000 points within continental Chile and extracted the classes that fell within
176 each point for LCChile, IGBP2013, and IGBP2014; we considered the point extracted from LCChile
177 as the truth and the values as the other two years as prediction
- 178 iii) calculate a confusion matrix with the classes extracted in the 1000 poitns for LCChile, IGBP2013, and
179 IGBP2014. Calculate the performance metrics of accuracy and F1.

$$\begin{aligned} \text{Accuracy} &= \frac{TP + TN}{TP + TN + FP + FN} = \frac{\text{correct classifications}}{\text{all classifications}} \\ \text{F1} &= \frac{2 \cdot TP}{2 \cdot TP + FP + FN} \end{aligned}$$

180 where TP and FN refer to true positive and false negative, correctly classified classes; TN and FP to true
181 negative and false positive, wrongly classified classes.

183 *3.4.2. Land cover persistence mask 2001-2022*

184 The time series of NDVI is affected by climatic conditions, vegetation development, seasonality, and changes
185 in vegetation type. In this study, we want to analyze the variation in vegetation productivity in different
186 land cover types and how it is affected by water demand, water supply, and soil moisture. In order to
187 avoid changes due to a change in the land cover type, that will wrongly impact NDVI. We will develop a
188 persistence mask for land cover for 2001–2023. Thereby, we reduce an important source of variation on a
189 regional scale.

190 Thus, we calculated a raster mask for IGBP MODIS considering the macroclasses that remain without
191 change for more than 80% of the years (2001–2022) per pixel, which allows us to identify the areas with no
192 land cover change for the macroclasses.

193 3.4.3. Land cover trend and drought indices

194 We calculated the surface occupied per land cover class into the five macrozones (“Norte Grande” to
195 “Austral”) per year for 2001–2023. After that, we calculated the trend’s change in surface; we used the Sen’
196 slope [62] based on Mann-Kendall [63]. This way, we obtain a matrix of trends of 5 x 5 (macrozones x land
197 cover). The aim is to later explore if the trend in land cover classes is associated with a trend in the drought
198 indices. For this, we will use the techniques of regression and regularization of Lasso [64] and Ridge [65].
199 Also, we will test random forests for this purpose [66]. We will choose the trend of land cover surface per
200 macroclass and macrozone as the response variable and the trend of the drought indices (SPI, SPEI, EDDI,
201 and SSI for time scales 1, 3, 6, 12, 24, and 36 months) as the predictor variables. With this analysis, we
202 expect to gather insights regarding whether there is a pattern of climatic influence along Chile or if what is
203 happening in Central Chile has to do with more localized climatic conditions.

204 3.5. Trend of drought indices for water demand and supply, soil moisture, and vegetation productivity

205 3.5.1. Mann-Kendall and Sen’s slope

206 To estimate if there are significant positive or negative trends for the drought indices, we used the non-
207 parametric test of Mann-Kendall [63]. To determine the magnitude of the trend, we used Sen’s slope [62].
208 Some of the advantages of applying this methodology are that the Sen’s slope is not affected by outliers as
209 regular regression does, and it is a non-parametric method that is not affected by the distribution of the
210 data. We applied both to the six time scales from 1981 to 2023 (monthly frequency) and the indices SPI,
211 EDDI, SPEI, and SSI. In the case of zcNDVI (six months) was for 2000 to 2023. Thus, we have 31 trends.
212 Also, we extracted the trend aggregated by macrozone and land cover class, obtaining a table of 31x5x5
213 (drought indices trends x macrozone x land cover class). We will use this data in Section 3.4 to analyze if
214 there is a strong relationship between the trends of drought indices and land cover surface within continental
215 Chile.

216 3.5.2. Trend in vegetation productivity without land cover change

217 [67] made a global analysis of the drought’s severity trend using SPI, SPEI, and the Standardized Evap-
218 otranspiration Deficit Index (SEDI; [68]) to evaluate AED. They indicate that the increase in hydrological
219 drought has been due to anthropogenic effects rather than climate change. This is because the global in-
220 crease in AED did not explain the change in the spatial pattern of the hydrological drought. Also, they state
221 that “*the increase in hydrological droughts has been primarily observed in regions with high water demand*
222 *and land cover change*”. We will contrast this hypothesis with what is occurring in Chile. To achieve this,
223 we will use the land cover class type that remains more than 80% of types for 2001–2022 to evaluate the
224 trend on zcNDVI and use this as a mask where there are low changes.

225 3.6. Impact for water supply and demand, and soil moisture in vegetation productivity within land cover
226 types

227 We analyze the drought indices of water demand and supply and soil moisture against vegetation to address:
228 i) if short- or long-term time scales are most important in impacting vegetation through Chile; and ii) the
229 strength of the correlation for the variable and the time scale. Then, we will summarize for each land cover
230 class and macrozone. Thus, we will be able to advance in understanding how climate is affecting vegetation,
231 considering the impact on the five macroclasses having vegetation: forest, cropland, grassland, savanna, and
232 shrubland.

233 To assess how water demand and supply and soil moisture are related to vegetation productivity (zcNDVI),
234 we analyze the linear correlation between the indices SPI, SPEI, EDDI, and SSI for 1, 3, 6, 12, 24, and 36-
235 month time scales against zcNDVI. We followed a similar approach to that used by [69] when using the SPI
236 for meteorological drought against the cumulative FAPAR (Fraction of Absorbed Photosynthetically Active

237 Radiation) as a proxy for vegetation productivity. We made a pixel-to-pixel linear correlation analysis per
 238 index. First, we calculate the Pearson coefficient of correlation for the six time scales and let the time scale
 239 that reaches the maximum correlation be significant ($p < 0.05$). Then, we extracted the Pearson correlation
 240 value corresponding to the time scales that reached the maximum value. Thus, we derived two raster maps
 241 per index, the first with the time scales and the second with the correlation value.

242 4. Results

243 4.1. Data

244 4.1.1. Validation of ERA5L variables

245 The average metrics of performance of ERA5L over the 266 weather stations were in the case of monthly
 246 temperature: $ubRMSE = 1.06^{\circ}C$, $MAE = 1.131^{\circ}C$, and $CC = 0.963$, showing a good agreement, low
 247 error, and low overestimation. For cumulative monthly precipitation, $MAE = 28.1\text{ mm}$, $bias = 1.93$, and
 248 $CC = 0.845$, showing a high correlation and a 93% bias and being overestimated by ERA5L. In the case of
 249 the 97 soil moisture stations, we averaged for the three depths (30, 60, and 90m) and then compared it with
 250 volumetric water content at 1m derived from ERA5L. For this case, we made a daily comparison, having
 251 a $CC = 0.71$, $RMSE = 0.174\text{ m}^3\text{ m}^{-3}$, $MAE = 0.167\text{ m}^3\text{ m}^{-3}$, and $bias = 1.74$. The ERA5 soil moisture
 252 overestimate is 74%, but it has a kind of good correlation.

253 4.2. LULC change for 2001-2022 and its relation with water supply and demand, and soil moisture

254 4.2.1. Land cover macroclases and validation

255 For vegetation, we obtained and use hereafter five macroclasses of land cover from IGBP MODIS: forest,
 256 shrubland, savanna, grassland, and croplands. Figure 1 c shows the spatial distribution of the macroclasses
 257 through Chile for the year 2022. The validation of IGBP2013 and IGBP2014 with LCChile reached near
 258 the same metrics of performance, having an accuracy of ~0.82 and a F1 score of ~0.66 (see SS1).

259 4.2.2. Land cover persistence mask 2001-2022

260 Figure 1 d, shows the macroclasses of land cover persistance (80%) during 2021-2022, respectively. Within
 261 continental Chile, forest is the vegetation type with highest surface with $135,00\text{ km}^2$, followed by grassland
 262 ($73,176\text{ km}^2$), savanna ($54,410\text{ km}^2$), shrubland ($24,959\text{ km}^2$), and cropland ($3,100\text{ km}^2$) (2). The macro-
 263 zones with major LULCC for 2001-2022 were “Centro”, “Sur”, and “Austral” with 36%, 31%, and 34%,
 264 respectively (Figure 1 and Table 3); of its surface that changes the type of land cover. Figure 2 shows the
 265 summary of the proportion of surface per land cover class and macrozone, derived from the persistance mask
 266 over continental Chile.

Table 2: Surface of the land cover class that persist during 2001-2022

Surface [km ²]						
macrozone	Forest	Cropland	Grassland	Savanna	Shrubland	Barren land
Norte Grande		873		7,796	169,244	
Norte Chico	88	4,221	580	16,085	83,059	
Centro	3,685	1,876	7,475	19,420	832	12,304
Sur	71,943	1,135	7,094	15,676		2,143
Austral	59,481		53,514	18,733	245	7,114

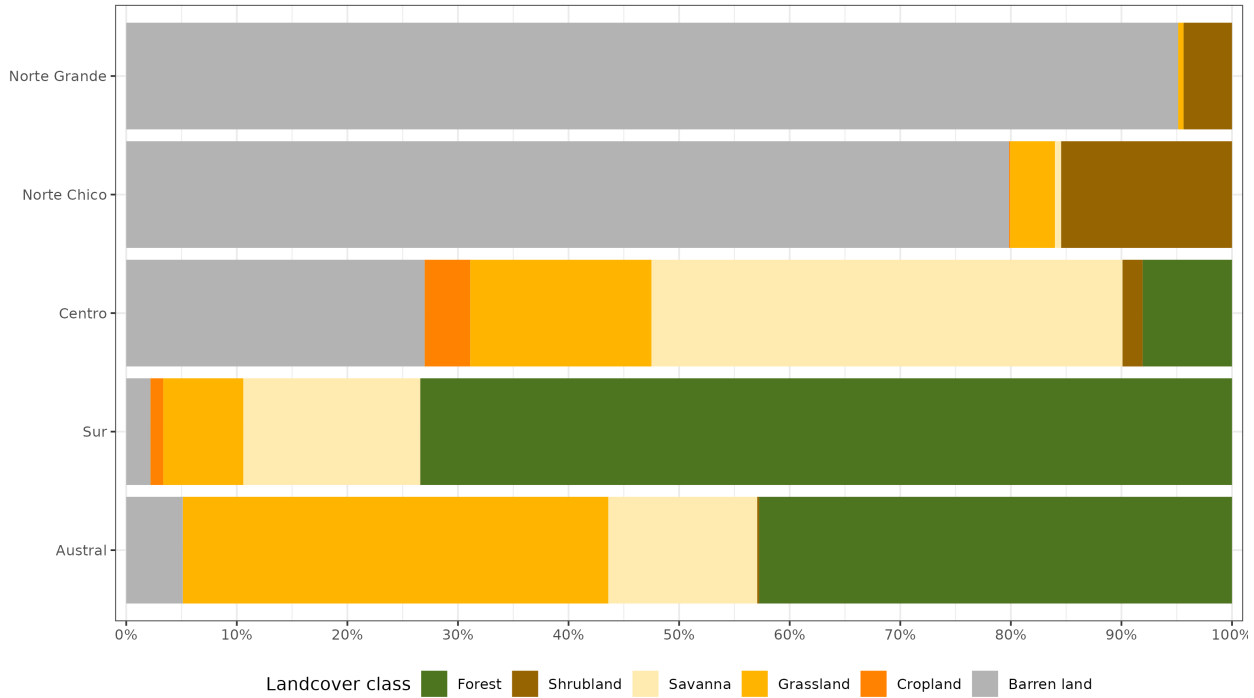
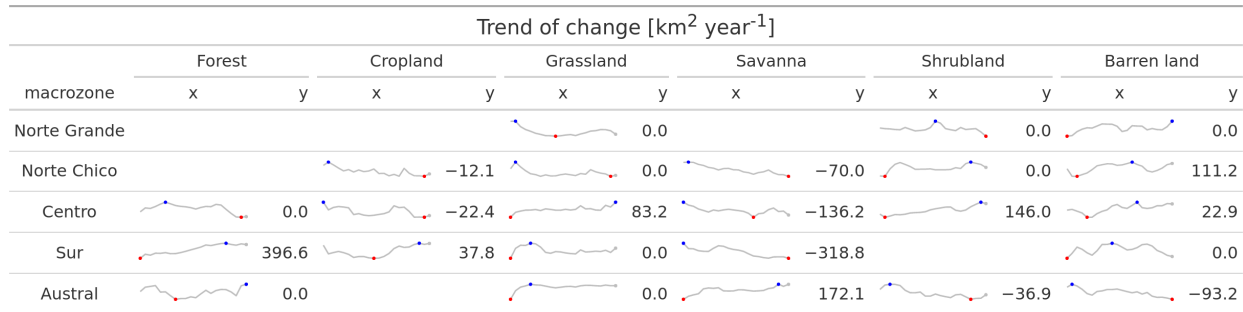


Figure 2: Proportion of land cover class from the persistent land cover for 2001-2022 ($>80\%$) per macrozone

Table 3: The value of Sen's slope trend next to the time-series plot of surface per land cover class (IGBP MCD12Q1.016) for 2001–2022 through Central Chile. Values of zero indicate that there was not a significant trend. Red dots on the plots indicate the maximum and minimum values of surface.



4.2.3. Land cover trend and drought indices

The “Norte Chico” shows an increase in barrend land of $111 \text{ km}^2 \text{year}^{-1}$ and a reduction in the class savanna of $70 \text{ km}^2 \text{year}^{-1}$. In the “Centro” and “Sur,” there are changes in the Chilean matorral, with an important reduction in savanna (136 to $318 \text{ km}^2 \text{yr}^{-1}$), and an increase in shrubland and grassland. Showing a change for more dense vegetation types. It appears to be a shift in the area of cropland from the “Centro” to the “Sur.” Also, there is a high increase in forest ($397 \text{ km}^2 \text{yr}^{-1}$) in the “Sur,” replacing the savanna lost.

Further, we want to address whether the trend in land cover change for 2001–2023 is associated with trends in drought indices of water demand and supply and/or soil moisture for macrozone and land cover macroclasses. From the three methods tested, Ridge, Lasso, and Random Forest, neither gives significant results regarding whether the trend in a drought index for any time scale explains the trend in land cover change. Nevertheless, in “Norte Chico” and “Centro,” there is a decrease in croplands and savanna and an

278 increase in barren land, which is associated with the variation in drought indices. Mainly for a decrease in
 279 water supply (SPI and SSI) and an increase in water demand (EDDI). However, due to the high variability
 280 from north to south in Chile, the climatic condition (arid, semi-arid, and humid), and the land cover type,
 281 we believe that only in those zones could the LULCC be driven to some degree by drought.

282 *4.3. Trend of drought indices for water demand and supply, soil moisture, and vegetation productivity*

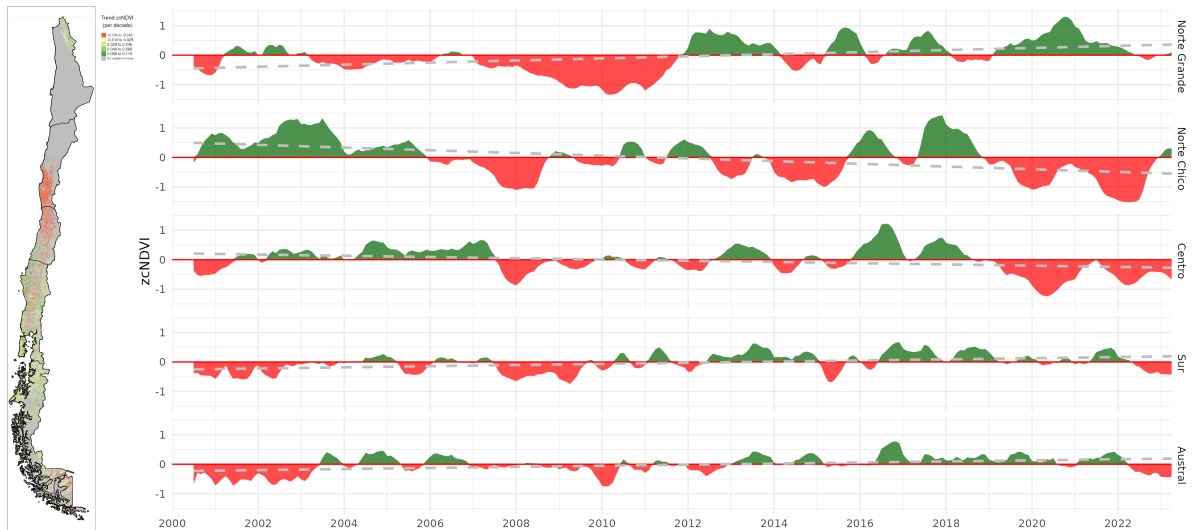


Figure 3: (a) Map of the linear trend of the index zcNDVI-6 for 2001–2023. Greener colors indicate a positive trend; redder colors correspond to a negative trend and a decrease in vegetation productivity. Grey colors indicate either no vegetation or a change in land cover type for 2001–2022. (b) Temporal variation of zcNDVI-6 aggregated at macrozone level within continental Chile. Each horizontal panel corresponds to a macrozone from ‘Norte Grande’ to ‘Austral’.

283 Regarding vegetation productivity aggregated through the macrozones in the five land cover macroclasses,
 284 in “Norte Grande,” there is an increase trend of 0.02 (z-index) per decade, related to types of grassland
 285 and shrubland. There is a negative trend in “Norte Chico” with -0.04 and “Centro” with -0.02 per decade.
 286 In the “Norte Chico,” savanna (-0.05) has the lowest trend, and the rest of the types are around -0.04.
 287 In “Centro,” shrubland reaches -0.06, grassland -0.05, and croplands and savanna -0.01 per decade. This
 288 could be associated either with a reduction in vegetation surface, a decrease in biomass, or browning [70].
 289 Vegetation reached its lowest values since the year 2019, reaching an extreme condition in early 2020 and
 290 2022 in the “Norte Chico” and Centro” (Mega Drought). The “Sur” and “Austral” show a positive trend
 291 of around 0.016 per decade (Figure 3). Despite the croplands suffering from drought just as badly as the
 292 native vegetation in “Norte Chico,” the Chilean matorral [18] appears to be the region most affected by a
 293 negative trend in vegetation productivity.

294 Analyzing the water supply, the macrozones that have the lowest trend are “Norte Chico” and “Centro,”
 295 where the SPI, SPEI, and SSI show that it decreases at longer time scales due to the prolonged reduction in
 296 precipitation. At 36 months, it reaches trends between -0.03 and -0.04 (z-score) per decade for SPI, SPEI,
 297 and SSI (Figure 5). For “Sur,” the behavior is similar, decreasing at longer scales and having between -0.016
 298 and -0.025 per decade for SPI, SPEI, and SSI. On the other hand, all macrozones show an increase in the
 299 trend in all the drought indices, with “Norte Grande” having the highest at 36 months (0.042 per decade).
 300 Because of this, the SPEI (which uses AED) reached its lowest value in “Norte Grande,” with -0.03 at 36
 301 months. Despite the other macrozones, “Austral” showed an increase in all indices, being the highest for
 302 EDDI at 36 months (0.025) and the lowest for SSI, which shows only a minor increase in the trend (Figure 5
 303 and Figure 4).

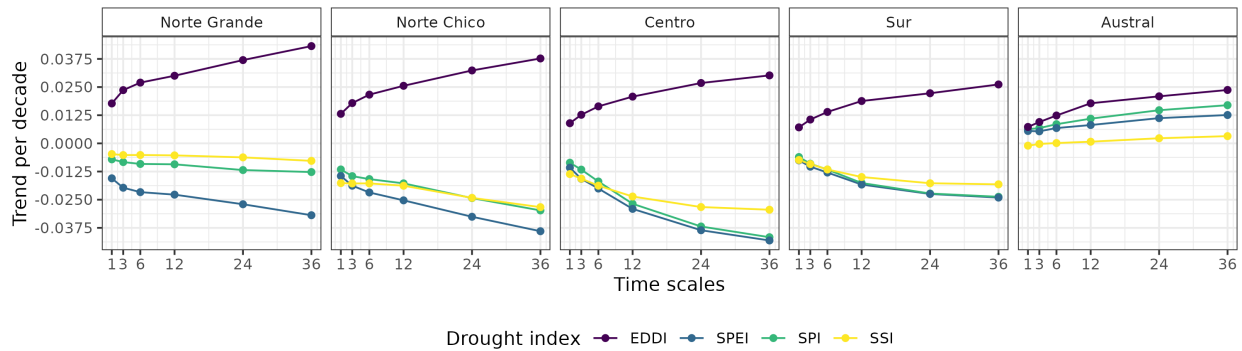


Figure 4: Trend per decade for the drought indices SPI, EDDI, SPEI, and SSI aggregated by macrozone.

304 4.4. Impact for water supply and demand, and soil moisture in vegetation productivity

305 According to what is shown in Figure 6, Figure 7, and Table 4, forest seems to be the most resistant type
 306 to drought. Showing that only “Centro” is slightly ($rsq = 0.25$) impacted by a 12-month soil moisture deficit
 307 (SSI-12). In the “Norte Chico” and to a lesser extent in the “Norte Grande,” it is evident that a SSI-12 with
 308 a $rsq = 0.45$ and a decrease in water supply (SPI-36 and SPEI-24 with $rsq = 0.28$ and 0.34 , respectively)
 309 have an impact on grasslands. However, this type was unaffected by soil moisture, water supply, or demand
 310 in macrozones further south. The types that show to be most affected by variation in climate conditions
 311 are shrublands, savannas, and croplands. For savannas in “Norte Chico,” the SSI-12 and SPI-24 reached
 312 an rsq of 0.74 and 0.58 , respectively. This value decreases to the south, but the SSI-12 is still the variable
 313 explaining more of the variation in vegetation productivity ($rsq = 0.45$ in “Centro” and 0.2 in “Sur”). In
 314 the case of croplands, the SPEI-12, SPI-36, and SSI-12 explain between 45% and 66% of “Norte Chico.”
 315 The type of land most impacted by climatic variation was shrubland, where soil moisture explained 59%
 316 and precipitation, 37% , in “Norte Chico” and “Centro,” with SSI-12 being the most relevant variable, then
 317 SPI-36 in “Norte Chico” and SPI-24 in “Sur.”

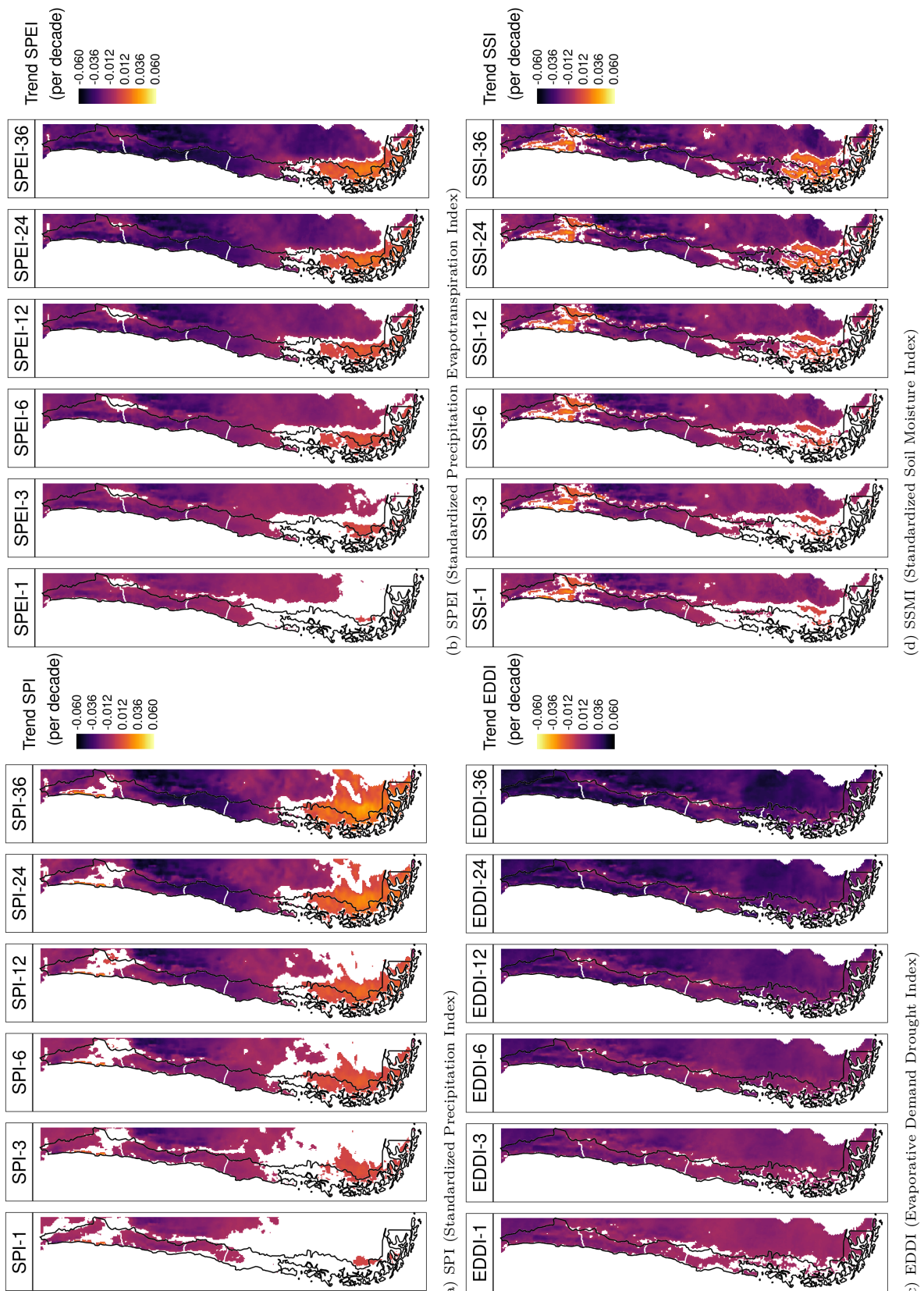


Figure 5: Linear trend of the drought index (*) at time scales of 1, 3, 6, 12, 24, and 36 months for 1981-2023

Table 4: Summary per land cover macroclass and macrozone regarding the correlation between zcNDVI with the drought indices EDDI, SPI, SPEI, and SSI for time scales of 1, 3, 6, 12, 24, and 36. The numbers in each cell indicate the time scale that reached the maximum correlation for the land cover and macrozone, and the color indicates the strength of the r-squared obtained with the index and the time scale.

	Forest				Cropland				Grassland				Savanna				Shrubland															
macrozone	EDDI	SPI	SPEI	SSI	EDDI	SPI	SPEI	SSI	EDDI	SPI	SPEI	SSI	EDDI	SPI	SPEI	SSI	EDDI	SPI	SPEI	SSI												
Norte Grande									36	36	36	12					36	12	36	12												
Norte Chico					36	36	12	12	36	36	24	12	36	24	24	12	36	36	24	12												
Centro	36	36	12	6	12	12	6	6	12	12	12	36	12	12	12	36	24	24	12													
Sur	36					6	6	6	6	6	6	12	6	6	6	6																
Austral	6	6									6	12	12	6	6	12																
 r-squared																																
0.2 0.4 0.6																																

318 5. Discussion

319 5.1. Drought trend and attribution to LULCC

320 [67], in a study at the global scale of drought trends, indicates that there have not been significant trends
 321 in meteorological drought since 1950. Also, state that the increase in hydrological trend in some parts of the
 322 globe (northeast Brazil and the Mediterranean region) is related to changes in land cover and specifically
 323 to the rapidly increasing irrigated area, which consequently increases water extraction. [71] analyzed the
 324 agricultural drought impact globally and in the main grain producer countries, finding that “since 1980, the
 325 Earth warming has not changed the drought area or intensity”.

326 In our study, we considered the variation in vegetation productivity in Chile for areas without changes
 327 in land cover macroclasses (see Section 4.2.2), to avoid misleading conclusions that could be related to the
 328 increase in water demand due to LULCC. Our results show a contrasting perspective. There has been
 329 a significant trend in the decline of vegetation productivity (zcNDVI) since 2000 for “Norte Chico” and
 330 “Centro,” which has been extreme between 2020 and 2022, seemingly due to an intense hydrological drought
 331 due to the persistence of the Mega Drought [10]. Despite using the persistence mask for vegetation’s trend
 332 analysis, cropland, which is the most water-demand type, showed a decrease trend in “Norte Chico” and
 333 “Centro.” Also, there was an increase in barren land for both types. These changes are associated with a
 334 decrease in water demand from vegetation. Nonetheless, we used the persistent landcover to ensure that
 335 the pixel has the same class; in the case of croplands, it could happen that some areas had changed crops
 336 for others with higher water consumption. But this effect should be minor compared to the results from
 337 landcover macroclasses.

338 On the other hand, for “Norte Chico” and “Centro,” our results show a decrease in trends of water supply
 339 (SPI and SSI), which are higher at larger time scales and consequently impact the hydrological system. We
 340 claim that what occurred in central Chile defies findings made at the global level [67, 71], demonstrating
 341 that a constant decrease in water supply rather than an increase in water demand (i.e., irrigated crops) is
 342 the main cause of the hydrological drought. Finally, central Chile has shown a diminishment in vegetation
 343 productivity for all macroclasses, mainly attributed to variation in water supply, i.e., precipitation, which
 344 could be strengthened by an increase in water demand by, for example, an increase in the surface area of
 345 irrigated crops.

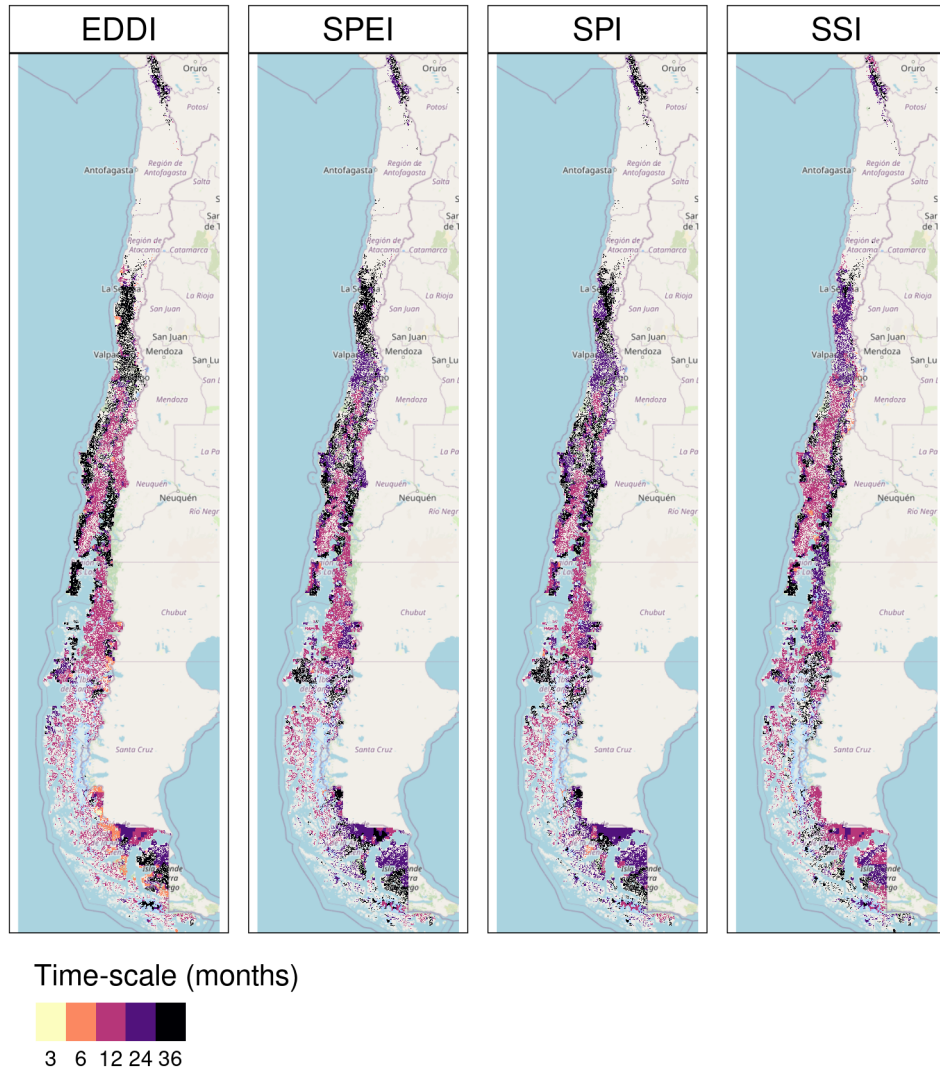


Figure 6: Time scales per drought index that reach the maximum coefficient of determination

346 5.2. Land cover types and their impact by drought

347 We found that shrubland, savannas (Chilean matorral), and croplands are the most sensitive to climate
 348 conditions. Being most affected by the 12-month soil moisture deficit. In a study in the Yangtze River
 349 Basin in China, Jiang2020 analyzed the impact of drought on vegetation using the SPEI and the Enhanced
 350 Vegetation Index (EVI). They found that cropland was more sensitive to drought than cropland, showing
 351 that cropland responds strongly to short- and medium-term drought (< SPEI-6). In our case, the SPEI-12
 352 was the one that most impacted the croplands in “Norte Chico” and “Centro.” In general, most studies show
 353 that croplands are most sensitive to short-term drought (< SPI-6) [13, 72, 73]. Short-term precipitation
 354 deficits impact soil water, and thus less water is available for plant growth. However, we found that in
 355 “Norte Chico,” an SPI-36 and SPEI-12 had a higher impact, which are associated with hydrological drought
 356 (long-term), and in “Centro,” an SPI-12 and SPEI-12. Thus, we attribute this impact to the hydrological
 357 drought that has decreased groundwater storage [74], which in turn is impacted by long-term deficits, and
 358 consequently, the vegetation is more dependent on groundwater. In “Sur” and “Austral,” the correlations
 359 between drought indices and vegetation productivity decrease, as do the time scales that reach the maximum

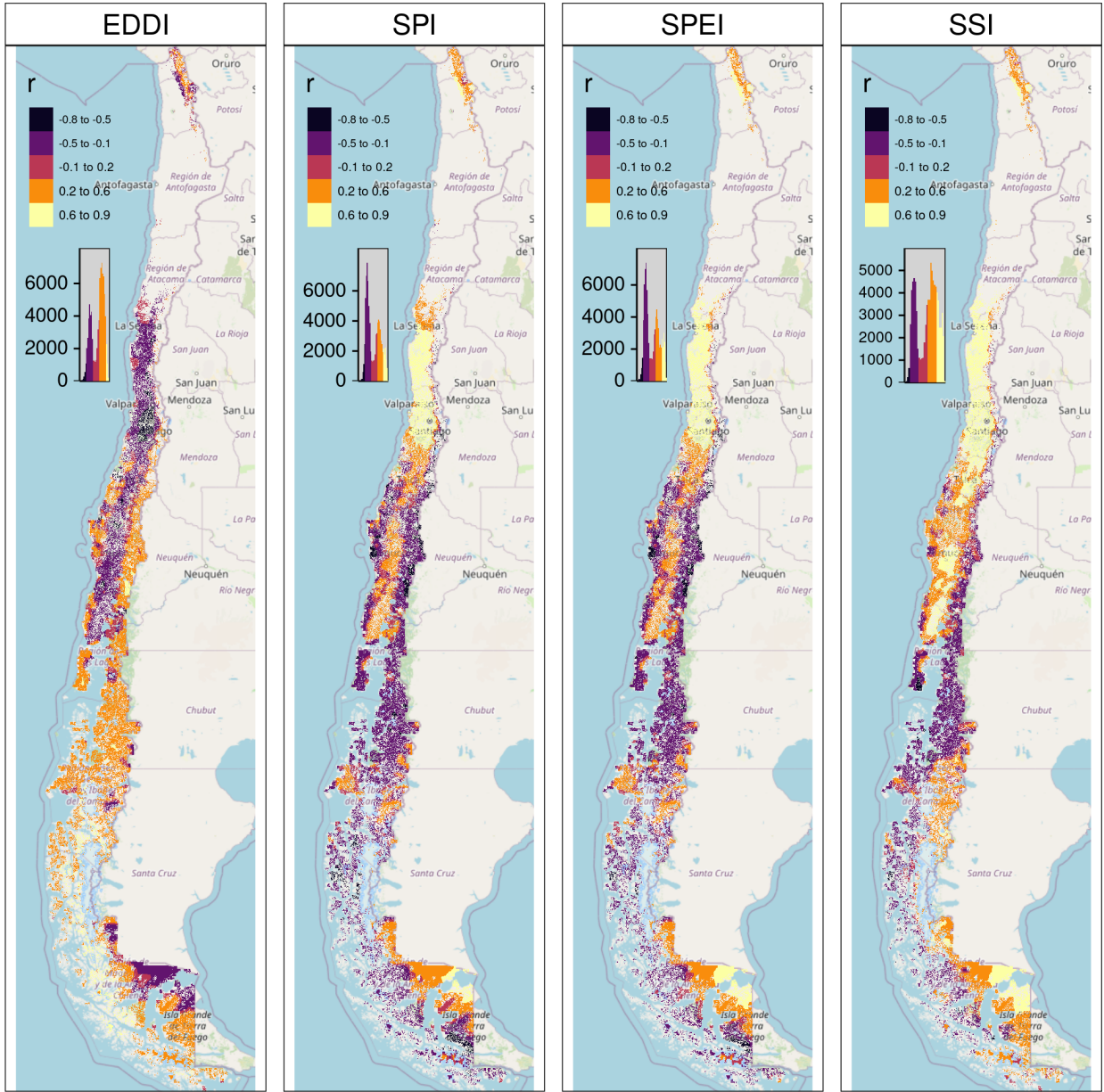


Figure 7: Pearson correlation value for the time scales and drought index that reach the maximum coefficient of determination

360 r-squared (4). What can be explained is that, south of “Centro,” predominate forest and grassland, the most
 361 resistant types. Also, drought episodes have been less frequent and intense. The drought episodes have had
 362 a lower impact on water availability for vegetation.

363 Extreme drought conditions are an important driver of tree mortality, as shown by [75] in Europe. However,
 364 we found that forest is the type of landcover macroclass less affected by variation in drought indices, being
 365 the most resistant landcover class to drought. Supporting this is [76], who asserts that Indian forests are
 366 the most drought-resistant and recover rapidly. Similarly, the work of [77], who analyzed vegetation loss
 367 and recovery in response to meteorological drought in the humid subtropical Pearl River basin in China,
 368 indicates that forests showed higher drought resistance. Using Vegetation Optical Depth (VOD), kNDVI,

369 and EVI, [78], tests the resistance of ecosystems and finds that ecosystems with more forests are better able
370 to handle severe droughts than croplands. They attribute the difference to a deeper rooting depth of trees,
371 a higher water storage capacity, and different water use strategies between forest and cropland [78].

372 In contrast to our observations, [79], who investigated *Cryptocarya alba* and *Beilschmiedia miersii* (both
373 members of the Lauraceae family) inhabiting sclerophyllous forests in Chile, concluded that the overall
374 development of the trees had decelerated, potentially indicating alterations in the inherent dynamics of
375 their respective forests. They attributed it to the cumulative effects of the unprecedented drought (i.e.,
376 hydrological drought). Thus, we attribute that forest to being the most resistant to drought, due to the fact
377 that most of the species comprising it are highly resilient to water scarcity compared to the other landcover
378 classes. Also, when we used MOD13A3 with a 1km spatial resolution to measure vegetation condition, it
379 took the average condition of 1 square kilometer. Then, to study how a type of forest (sclerophyllous forest)
380 changes in response to drought on a local level using remote sensing, we should use operational products
381 with higher spatial resolutions, such as those from Landsat or Sentinel, which can show how different the
382 forests are.

383 5.3. *Soil moisture, vegetation productivity, and agricultural drought.*

384 The main external factors that affect biomass production by vegetation are ET and SM, and the rate
385 of ET in turn depends on the availability of water storage in the root zone. Thus, soil moisture plays
386 a key role in land carbon uptake and, consequently, in the production of biomass [80]. Moreover, [81]
387 indicates there is a bidirectional causality between soil moisture and vegetation productivity. For this, lastly,
388 some studies have redefined agricultural drought as soil moisture drought from the hydrological perspective
389 [7, 82]. Even though soil moisture is the external factor most determinant of vegetation biomass, there
390 are multiple internal factors, such as species, physiological characteristics, and plant hydraulics, that would
391 affect vegetation productivity. Because of that, we believe that agricultural drought, referring to the drought
392 that impacts vegetation productivity, is the most proper term, as originally defined by [6].

393 Our results showed that the drought index derived from soil moisture (SSI) was the most effective in
394 explaining vegetation productivity within landcover macroclasses. However, there is strong spatial variability
395 throughout Chile and between classes, mainly attributable to climate heterogeneity, hydrological status, or
396 vegetation resistance to water scarcity. The semi-arid “Norte Chico” and the Mediterranean “Centro” were
397 where SSI had the best performance. Medium-term deficits of 12 months are more relevant in the response
398 of vegetation, which decreases to the south, and in the case of croplands, they seem to react in a shorter
399 time, with six months (SSI-6) in “Centro.”

400 [83]

401 5.4. *Drought indices of water demand and supply, soil moisture to predict changes in vegetation productivity*

402 3. Como podrían servir estos resultados para desarrollar o mejorar un predictor de productividad de la
403 vegetación.

- 404 • Los datos ERA5L están casi en tiempo real, 7 días; MODIS también.
405 • EL SSI se ve como un poderoso indicador que explica la variabilidad en la productividad de la veg-
406 etación.

407 5.5. *Early drought forecasting*

408 5.6. *Future outlook*

409 4.- Qué se podría hacer mejor en futuras investigaciones del tema. - mejorar la resolución y calidad de los
410 datos climáticos -

411 6. Conclusion

412 **References**

- [1] K. Calvin, D. Dasgupta, G. Krinner, A. Mukherji, P. W. Thorne, C. Trisos, J. Romero, P. Aldunce, K. Barrett, G. Blanco, W. W. Cheung, S. Connors, F. Denton, A. Diougue-Niang, D. Dodman, M. Garschagen, O. Geden, B. Hayward, C. Jones, F. Jotzo, T. Krug, R. Lasco, Y.-Y. Lee, V. Masson-Delmotte, M. Meinshausen, K. Mintenbeck, A. Mokssit, F. E. Otto, M. Pathak, A. Pirani, E. Poloczanska, H.-O. Pörtner, A. Revi, D. C. Roberts, J. Roy, A. C. Ruane, J. Skea, P. R. Shukla, R. Slade, A. Slangen, Y. Sokona, A. A. Sörensson, M. Tignor, D. Van Vuuren, Y.-M. Wei, H. Winkler, P. Zhai, Z. Zommers, J.-C. Hourcade, F. X. Johnson, S. Pachauri, N. P. Simpson, C. Singh, A. Thomas, E. Totin, P. Arias, M. Bustamante, I. Elgizouli, G. Flato, M. Howden, C. Méndez-Vallejo, J. J. Pereira, R. Pichs-Madruga, S. K. Rose, Y. Saheb, R. Sánchez Rodríguez, D. Ürge Vorsatz, C. Xiao, N. Yassa, A. Alegria, K. Armour, B. Bednar-Friedl, K. Blok, G. Cissé, F. Dentener, S. Eriksen, E. Fischer, G. Garner, C. Guivarch, M. Haasnoot, G. Hansen, M. Hauser, E. Hawkins, T. Hermans, R. Kopp, N. Leprince-Ringuet, J. Lewis, D. Ley, C. Ludden, L. Niamir, Z. Nicholls, S. Some, S. Szopa, B. Trewhin, K.-I. Van Der Wijst, G. Winter, M. Witting, A. Birt, M. Ha, J. Romero, J. Kim, E. F. Haites, Y. Jung, R. Stavins, A. Birt, M. Ha, D. J. A. Orendain, L. Ignon, S. Park, Y. Park, A. Reisinger, D. Cammaramo, A. Fischlin, J. S. Fuglestvedt, G. Hansen, C. Ludden, V. Masson-Delmotte, J. R. Matthews, K. Mintenbeck, A. Pirani, E. Poloczanska, N. Leprince-Ringuet, C. Péan, *IPCC, 2023: Climate Change 2023: Synthesis Report. Contribution of Working Groups I, II and III to the Sixth Assessment Report of the Intergovernmental Panel on Climate Change [Core Writing Team, H. Lee and J. Romero (eds.)]*. IPCC, Geneva, Switzerland., Tech. rep., Intergovernmental Panel on Climate Change (IPCC) (Jul. 2023).
URL <https://www.ipcc.ch/report/ar6/syr/>
- [2] IPCC, *Climate Change 2013: The Physical Science Basis. Contribution of Working Group I to the Fifth Assessment Report of the Intergovernmental Panel on Climate Change*, Cambridge University Press, Cambridge, UK; New York, USA, 2013. doi:[10.1017/CBO9781107415324](https://doi.org/10.1017/CBO9781107415324).
URL www.climatechange2013.org
- [3] X. a. A. M. a. B. W. a. D. C. a. L. A. a. G. S. a. I. I. a. K. J. a. L. S. a. O. F. a. P. I. a. S. M. a. V.-S. S. a. W. M. a. Z. . M.-D. B. a. V. a. O. Seneviratne, S and Zhang, *Weather and Climate Extreme Events in a Changing Climate*, Cambridge University Press. In Press., 2021, publication Title: *Climate Change 2021: The Physical Science Basis. Contribution of Working Group I to the Sixth Assessment Report of the Intergovernmental Panel on Climate Change*.
- [4] S. D. Crasubay, A. R. Ramirez, S. L. Carter, M. S. Cross, K. R. Hall, D. J. Bathke, J. L. Betancourt, S. Colt, A. E. Cravens, M. S. Dalton, J. B. Dunham, L. E. Hay, M. J. Hayes, J. McEvoy, C. A. McNutt, M. A. Moritz, K. H. Nislow, N. Raheem, T. Sanford, *Defining Ecological Drought for the Twenty-First Century*, Bulletin of the American Meteorological Society 98 (12) (2017) 2543–2550, publisher: American Meteorological Society. doi:[10.1175/BAMS-D-16-0292.1](https://doi.org/10.1175/BAMS-D-16-0292.1).
URL <https://journals.ametsoc.org/view/journals/bams/98/12/bams-d-16-0292.1.xml>
- [5] L. Luo, D. Apps, S. Arcand, H. Xu, M. Pan, M. Hoerling, *Contribution of temperature and precipitation anomalies to the California drought during 2012–2015*, Geophysical Research Letters 44 (7) (2017) 3184–3192. doi:[10.1002/2016GL072027](https://doi.org/10.1002/2016GL072027).
URL <https://agupubs.onlinelibrary.wiley.com/doi/10.1002/2016GL072027>
- [6] D. A. Wilhite, M. H. Glantz, *Understanding: The drought phenomenon: The role of definitions*, Water International 10 (3) (1985) 111–120. doi:[10.1080/02508068508686328](https://doi.org/10.1080/02508068508686328).
URL <http://dx.doi.org/10.1080/02508068508686328>
- [7] A. F. Van Loon, T. Gleeson, J. Clark, A. I. Van Dijk, K. Stahl, J. Hannaford, G. Di Baldassarre, A. J. Teuling, L. M. Tallaksen, R. Uijlenhoet, D. M. Hannah, J. Sheffield, M. Svoboda, B. Verbeiren, T. Wagener, S. Rangecroft, N. Wanders, H. A. Van Lanen, *Drought in the Anthropocene*, Nature Geoscience 9 (2) (2016) 89–91. doi:[10.1038/ngeo2646](https://doi.org/10.1038/ngeo2646).
- [8] A. AghaKouchak, A. Mirchi, K. Madani, G. Di Baldassarre, A. Nazemi, A. Alborzi, H. Anjileli, M. Azarderakhsh, F. Chiang, E. Hassanzadeh, L. S. Huning, I. Mallakpour, A. Martinez, O. Mazdiyasni, H. Moftakhari, H. Norouzi, M. Sadegh, D. Sadeqi, A. F. Van Loon, N. Wanders, *Anthropogenic Drought: Definition, Challenges, and Opportunities*, Reviews of Geophysics 59 (2) (2021) e2019RG000683. doi:[10.1029/2019RG000683](https://doi.org/10.1029/2019RG000683).
URL <https://agupubs.onlinelibrary.wiley.com/doi/10.1029/2019RG000683>
- [9] I. J. Slette, A. K. Post, M. Awad, T. Even, A. Punzalan, S. Williams, M. D. Smith, A. K. Knapp, *How ecologists define drought, and why we should do better*, Global Change Biology 25 (10) (2019) 3193–3200. doi:[10.1111/gcb.14747](https://doi.org/10.1111/gcb.14747).
URL <https://onlinelibrary.wiley.com/doi/10.1111/gcb.14747>
- [10] R. Garreaud, C. Alvarez-Garreton, J. Barichivich, J. P. Boisier, D. Christie, M. Galleguillos, C. LeQuesne, J. McPhee, M. Zambrano-Bigiarini, *The 2010–2015 mega drought in Central Chile: Impacts on regional hydroclimate and vegetation*, Hydrology and Earth System Sciences Discussions 2017 (2017) 1–37. doi:[10.5194/hess-2017-191](https://doi.org/10.5194/hess-2017-191).
URL <http://www.hydrol-earth-syst-sci-discuss.net/hess-2017-191/>
- [11] F. Zambrano, Four decades of satellite data for agricultural drought monitoring throughout the growing season in Central Chile, in: R. M. Vijay P. Singh Deepak Jhajharia, R. Kumar (Eds.), *Integrated Drought Management*, Two Volume Set, CRC Press, 2023, p. 28.
- [12] J. P. Boisier, C. Alvarez-Garreton, R. R. Cordero, A. Damiani, L. Gallardo, R. D. Garreaud, F. Lambert, C. Ramallo, M. Rojas, R. Rondanelli, *Anthropogenic drying in central-southern Chile evidenced by long-term observations and climate model simulations*, Elementa 6 (1) (2018) 74. doi:[10.1525/elementa.328](https://doi.org/10.1525/elementa.328).
URL <https://www.elementascience.org/article/10.1525/elementa.328/>
- [13] F. Zambrano, M. Lillo-Saavedra, K. Verbist, O. Lagos, *Sixteen years of agricultural drought assessment of the biobío region in chile using a 250 m resolution vegetation condition index (VCI)*, Remote Sensing 8 (6) (2016) 1–20, publisher: Multidisciplinary Digital Publishing Institute. doi:[10.3390/rs8060530](https://doi.org/10.3390/rs8060530).
URL <http://www.mdpi.com/2072-4292/8/6/530>

- 476 [14] F. Zambrano, A. Vrieling, A. Nelson, M. Meroni, T. Tadesse, [Prediction of drought-induced reduction of agricultural](#)
 477 [productivity in Chile from MODIS, rainfall estimates, and climate oscillation indices](#), Remote Sensing of Environment 219
 478 (2018) 15–30, publisher: Elsevier. [doi:10.1016/j.rse.2018.10.006](#).
 479 URL <https://www.sciencedirect.com/science/article/pii/S0034425718304541>
- 480 [15] A. Miranda, A. Lara, A. Altamirano, C. Di Bella, M. E. González, J. Julio Camarero, [Forest browning trends in response](#)
 481 [to drought in a highly threatened mediterranean landscape of South America](#), Ecological Indicators 115 (2020) 106401.
 482 [doi:10.1016/j.ecolind.2020.106401](#).
 483 URL <https://linkinghub.elsevier.com/retrieve/pii/S1470160X20303381>
- 484 [16] A. Venegas-González, F. R. Juñent, A. G. Gutiérrez, M. T. Filho, [Recent radial growth decline in response to increased](#)
 485 [drought conditions in the northernmost Nothofagus populations from South America](#), Forest Ecology and Management
 486 409 (2018) 94–104. [doi:10.1016/j.foreco.2017.11.006](#).
 487 URL <https://linkinghub.elsevier.com/retrieve/pii/S0378112717313993>
- 488 [17] R. Urrutia-Jalabert, M. E. González, . González-Reyes, A. Lara, R. Garreaud, [Climate variability and forest fires in](#)
 489 [central and south-central Chile](#), Ecosphere 9 (4) (2018) e02171. [doi:10.1002/ecs2.2171](#).
 490 URL <https://esajournals.onlinelibrary.wiley.com/doi/10.1002/ecs2.2171>
- 491 [18] I. Fuentes, R. Fuster, D. Avilés, W. Vervoort, [Water scarcity in central Chile: the effect of climate and land cover changes](#)
 492 [on hydrologic resources](#), Hydrological Sciences Journal 66 (6) (2021) 1028–1044. [doi:10.1080/02626667.2021.1903475](#).
 493 URL <https://www.tandfonline.com/doi/full/10.1080/02626667.2021.1903475>
- 494 [19] C. Alvarez-Garreton, J. P. Boisier, R. Garreaud, J. Seibert, M. Vis, [Progressive water deficits during multiyear droughts](#)
 495 [in basins with long hydrological memory in Chile](#), Hydrology and Earth System Sciences 25 (1) (2021) 429–446. [doi:](#)
 496 [10.5194/hess-25-429-2021](#).
 497 URL <https://hess.copernicus.org/articles/25/429/2021/>
- 498 [20] F. J. Fernández, F. Vásquez-Lavín, R. D. Ponce, R. Garreaud, F. Hernández, O. Link, F. Zambrano, M. Hanemann, [The](#)
 499 [economics impacts of long-run droughts: Challenges, gaps, and way forward](#), Journal of Environmental Management 344
 500 (2023) 118726. [doi:10.1016/j.jenvman.2023.118726](#).
 501 URL <https://linkinghub.elsevier.com/retrieve/pii/S0301479723015141>
- 502 [21] J. Muñoz-Sabater, E. Dutra, A. Agustí-Panareda, C. Albergel, G. Arduini, G. Balsamo, S. Boussetta, M. Choulga,
 503 S. Harrigan, H. Hersbach, B. Martens, D. G. Miralles, M. Piles, N. J. Rodríguez-Fernández, E. Zsoter, C. Buontempo,
 504 J.-N. Thépaut, [ERA5-Land: a state-of-the-art global reanalysis dataset for land applications](#), Earth System Science Data
 505 13 (9) (2021) 4349–4383. [doi:10.5194/essd-13-4349-2021](#).
 506 URL <https://essd.copernicus.org/articles/13/4349/2021/>
- 507 [22] M. Nouri, [Drought Assessment Using Gridded Data Sources in Data-Poor Areas with Different Aridity Conditions](#), Water
 508 Resources Management 37 (11) (2023) 4327–4343. [doi:10.1007/s11269-023-03555-4](#).
 509 URL <https://link.springer.com/10.1007/s11269-023-03555-4>
- 510 [23] M. Wang, L. Menzel, S. Jiang, L. Ren, C.-Y. Xu, H. Cui, [Evaluation of flash drought under the impact of heat wave events](#)
 511 [in southwestern Germany](#), Science of The Total Environment 904 (2023) 166815. [doi:10.1016/j.scitotenv.2023.166815](#).
 512 URL <https://linkinghub.elsevier.com/retrieve/pii/S0048969723054402>
- 513 [24] H. West, N. Quinn, M. Horswell, [Remote sensing for drought monitoring \& impact assessment: Progress, past challenges](#)
 514 [and future opportunities](#), Remote Sensing of Environment 232, publisher: Elsevier Inc. (Oct. 2019). [doi:10.1016/j.rse.2019.111291](#).
- 515 [25] A. AghaKouchak, A. Farahmand, F. S. Melton, J. Teixeira, M. C. Anderson, B. D. Wardlow, C. R. Hain, [Remote](#)
 516 [sensing of drought: Progress, challenges and opportunities](#), Reviews of Geophysics 53 (2) (2015) 452–480. [doi:10.1002/2014RG000456](#).
 517 URL <http://dx.doi.org/10.1002/2014RG000456>.
- 518 [26] J. M. Paruelo, M. Texeira, L. Staiano, M. Mastrángelo, L. Amdan, F. Gallego, [An integrative index of Ecosystem Services](#)
 519 [provision based on remotely sensed data](#), Ecological Indicators 71 (2016) 145–154, publisher: Elsevier. [doi:10.1016/J.ECOLIND.2016.06.054](#).
 520 URL <https://www.sciencedirect.com/science/article/pii/S1470160X16303843>
- 521 [27] A. Schucknecht, M. Meroni, F. Kayitakire, A. Boureima, A. Schucknecht, M. Meroni, F. Kayitakire, A. Boureima,
 522 [Phenology-Based Biomass Estimation to Support Rangeland Management in Semi-Arid Environments](#), Remote Sensing
 523 9 (5) (2017) 463, publisher: Multidisciplinary Digital Publishing Institute. [doi:10.3390/rs9050463](#).
 524 URL <http://www.mdpi.com/2072-4292/9/5/463>
- 525 [28] H. T. Tran, J. B. Campbell, R. H. Wynne, Y. Shao, S. V. Phan, [Drought and Human Impacts on Land Use and Land](#)
 526 [Cover Change in a Vietnamese Coastal Area](#), Remote Sensing 2019, Vol. 11, Page 333 11 (3) (2019) 333, publisher:
 527 Multidisciplinary Digital Publishing Institute. [doi:10.3390/RS11030333](#).
 528 URL <https://www.mdpi.com/2072-4292/11/3/333.htm>
- 529 [29] F. O. Akinyemi, [Vegetation Trends, Drought Severity and Land Use-Land Cover Change during the Growing Season](#)
 530 [in Semi-Arid Contexts](#), Remote Sensing 2021, Vol. 13, Page 836 13 (5) (2021) 836, publisher: Multidisciplinary Digital
 531 Publishing Institute. [doi:10.3390/RS13050836](#).
 532 URL <https://www.mdpi.com/2072-4292/13/5/836.htm>
- 533 [30] G. Grekousis, G. Mountarakis, M. Kavouras, [An overview of 21 global and 43 regional land-cover mapping products](#),
 534 International Journal of Remote Sensing 36 (21) (2015) 5309–5335. [doi:10.1080/01431161.2015.1093195](#).
 535 URL <https://www.tandfonline.com/doi/full/10.1080/01431161.2015.1093195>
- 536 [31] M. Friedl, D. Sulla-Menashe, MCD12Q1 MODIS/Terra+Aqua Land Cover Type Yearly L3 Global 500m SIN Grid V006
 537 [Data set]. NASA EOSDIS Land Processes DAAC (2019). [doi:10.5067/MODIS/MCD12Q1.006](#).

- 541 [32] M. Ahmed, M. Sultan, J. Wahr, E. Yan, The use of GRACE data to monitor natural and anthropogenic induced variations
 542 in water availability across Africa, *Earth-Science Reviews* 136 (2014) 289–300, publisher: Elsevier. [doi:10.1016/J.EARSCIREV.2014.05.009](https://doi.org/10.1016/J.EARSCIREV.2014.05.009).
- 543 [33] S. Ma, Q. Wu, J. Wang, S. Zhang, **Temporal Evolution of Regional Drought Detected from GRACE TWSA and CCI**
 544 **SM in Yunnan Province, China**, *Remote Sensing* 2017, Vol. 9, Page 1124 9 (11) (2017) 1124, publisher: Multidisciplinary
 545 Digital Publishing Institute. [doi:10.3390/RS9111124](https://doi.org/10.3390/RS9111124).
 546 URL <https://www.mdpi.com/2072-4292/9/11/1124/htm>
- 547 [34] WMO, M. Svoboda, M. Hayes, D. A. Wood, **Standardized Precipitation Index User Guide**, WMO, Geneva, 2012, series
 548 Title: WMO Publication Title: WMO-No. 1090 © Issue: 1090.
 549 URL http://library.wmo.int/opac/index.php?lvl=notice_display&id=13682
- 550 [35] T. B. McKee, N. J. Doesken, J. Kleist, The relationship of drought frequency and duration to time scales. In: Proceedings
 551 of the Ninth Conference on Applied Climatology., American Meteorological Society (Boston) (1993) 179–184.
- 552 [36] S. M. Vicente-Serrano, S. Beguería, J. I. López-Moreno, **A multiscalar drought index sensitive to global warming: The stan-**
 553 **dardized precipitation evapotranspiration index**, *Journal of Climate* 23 (7) (2010) 1696–1718. [doi:10.1175/2009JCLI2909.1](https://doi.org/10.1175/2009JCLI2909.1)
 554 URL <http://dx.doi.org/10.1175/2009JCLI2909.1>
- 555 [37] M. T. Hobbins, A. Wood, D. J. McEvoy, J. L. Huntington, C. Morton, M. Anderson, C. Hain, **The Evaporative Demand**
 556 **Drought Index. Part I: Linking Drought Evolution to Variations in Evaporative Demand**, *Journal of Hydrometeorology*
 557 17 (6) (2016) 1745–1761. [doi:10.1175/JHM-D-15-0121.1](https://doi.org/10.1175/JHM-D-15-0121.1).
 558 URL <http://journals.ametsoc.org/doi/10.1175/JHM-D-15-0121.1>
- 559 [38] D. J. McEvoy, J. L. Huntington, M. T. Hobbins, A. Wood, C. Morton, M. Anderson, C. Hain, **The Evaporative Demand**
 560 **Drought Index. Part II: CONUS-Wide Assessment against Common Drought Indicators**, *Journal of Hydrometeorology*
 561 17 (6) (2016) 1763–1779. [doi:10.1175/JHM-D-15-0122.1](https://doi.org/10.1175/JHM-D-15-0122.1).
 562 URL <http://journals.ametsoc.org/doi/10.1175/JHM-D-15-0122.1>
- 563 [39] B. Narasimhan, R. Srinivasan, Development and evaluation of Soil Moisture Deficit Index (SMDI) and Evapotranspiration
 564 Deficit Index (ETDI) for agricultural drought monitoring, *Agricultural and Forest Meteorology* 133 (1-4) (2005) 69–88.
 565 [doi:10.1016/j.agrformet.2005.07.012](https://doi.org/10.1016/j.agrformet.2005.07.012).
 566 URL <https://linkinghub.elsevier.com/retrieve/pii/S0168192305001565>
- 567 [40] A. G. S. S. Souza, A. Ribeiro Neto, L. L. D. Souza, **Soil moisture-based index for agricultural drought assessment: SMADI**
 568 **application in Pernambuco State-Brazil**, *Remote Sensing of Environment* 252 (2021) 112124. [doi:10.1016/j.rse.2020.112124](https://doi.org/10.1016/j.rse.2020.112124).
 569 URL <https://linkinghub.elsevier.com/retrieve/pii/S0034425720304971>
- 570 [41] F. N. Kogan, Application of vegetation index and brightness temperature for drought detection, *Advances in Space*
 571 *Research* 15 (11) (1995) 91–100. [doi:10.1016/0273-1177\(95\)00079-T](https://doi.org/10.1016/0273-1177(95)00079-T).
- 572 [42] A. Cui, J. Li, Q. Zhou, R. Zhu, H. Liu, G. Wu, Q. Li, **Use of a multiscalar GRACE-based standardized terrestrial water**
 573 **storage index for assessing global hydrological droughts**, *Journal of Hydrology* 603 (2021) 126871. [doi:10.1016/j.jhydrol.2021.126871](https://doi.org/10.1016/j.jhydrol.2021.126871).
 574 URL <https://linkinghub.elsevier.com/retrieve/pii/S0022169421009215>
- 575 [43] P. Aceituno, J. P. Boisier, R. Garreaud, R. Rondanelli, J. A. Rutllant, **Climate and Weather in Chile**, in: B. Fernández,
 576 J. Gironás (Eds.), *Water Resources of Chile*, Vol. 8, Springer International Publishing, Cham, 2021, pp. 7–29.
 577 URL https://link.springer.com/10.1007/978-3-030-56901-3_2
- 578 [44] R. D. Garreaud, **The Andes climate and weather**, *Advances in Geosciences* 22 (2009) 3–11. [doi:10.5194/adgeo-22-3-2009](https://doi.org/10.5194/adgeo-22-3-2009).
 579 URL <https://adgeo.copernicus.org/articles/22/3/2009/>
- 580 [45] H. E. Beck, T. R. McVicar, N. Vergopolan, A. Berg, N. J. Lutsko, A. Dufour, Z. Zeng, X. Jiang, A. I. J. M. van Dijk, D. G.
 581 Miralles, **High-resolution (1 km) Köppen-Geiger maps for 1901–2099 based on constrained CMIP6 projections**, *Scientific*
 582 *Data* 10 (1) (Oct. 2023). [doi:10.1038/s41597-023-02549-6](https://doi.org/10.1038/s41597-023-02549-6).
 583 URL <https://dx.doi.org/10.1038/s41597-023-02549-6>
- 584 [46] R Core Team, **R: A Language and Environment for Statistical Computing**, R Foundation for Statistical Computing,
 585 Vienna, Austria, 2023.
 586 URL <https://www.R-project.org/>
- 587 [47] K. Hufkens, R. Stauffer, E. Campitelli, **The ecwmfr package: an interface to ECMWF API endpoints** (2019).
 588 URL <https://bluegreen-labs.github.io/ecwmfr/>
- 589 [48] R. J. Hijmans, **terra: Spatial Data Analysis**, 2023.
 590 URL <https://CRAN.R-project.org/package=terra>
- 591 [49] E. Pebesma, R. Bivand, **Spatial Data Science: With applications in R**, Chapman and Hall/CRC, London, 2023.
 592 URL <https://r-spatial.org/book/>
- 593 [50] E. Pebesma, **Simple Features for R: Standardized Support for Spatial Vector Data**, *The R Journal* 10 (1) (2018) 439–446.
 594 [doi:10.32614/RJ-2018-009](https://doi.org/10.32614/RJ-2018-009).
 595 URL <https://doi.org/10.32614/RJ-2018-009>
- 596 [51] S. Beguería, S. M. Vicente-Serrano, **SPEI: Calculation of the Standardized Precipitation-Evapotranspiration Index**, 2023.
 597 URL <https://CRAN.R-project.org/package=SPEI>
- 598 [52] K. Didan, MOD13Q1 MODIS/Terra Vegetation Indices 16-Day L3 Global 250m SIN Grid V006, Tech. rep., NASA EOSDIS
 599 Land Processes DAAC (2015). [doi:https://dx.doi.org/10.5067/MODIS/MOD13Q1.006](https://dx.doi.org/10.5067/MODIS/MOD13Q1.006).
- 600 [53] G. H. Hargreaves, **Defining and Using Reference Evapotranspiration**, *Journal of Irrigation and Drainage Engineering*
 601 120 (6) (1994) 1132–1139. [doi:10.1061/\(ASCE\)0733-9437\(1994\)120:6\(1132\)](https://doi.org/10.1061/(ASCE)0733-9437(1994)120:6(1132)).

- 606 URL <https://ascelibrary.org/doi/10.1061/%28ASCE%290733-9437%281994%29120%3A6%281132%29>
- 607 [54] G. H. Hargreaves, Z. A. Samani, Reference crop evapotranspiration from temperature, Applied engineering in agriculture
608 1 (2) (1985) 96–99.
- 609 [55] S. M. Vicente-Serrano, C. Azorin-Molina, A. Sanchez-Lorenzo, J. Revuelto, J. I. López-Moreno, J. C. González-Hidalgo,
610 E. Moran-Tejeda, F. Espejo, **Reference evapotranspiration variability and trends in Spain, 1961–2011**, Global and Planetary
611 Change 121 (2014) 26–40. doi:[10.1016/j.gloplacha.2014.06.005](https://doi.org/10.1016/j.gloplacha.2014.06.005).
- 612 URL <https://linkinghub.elsevier.com/retrieve/pii/S0921818114001180>
- 613 [56] Z. Hao, A. AghaKouchak, Multivariate Standardized Drought Index: A parametric multi-index model, Advances in Water
614 Resources 57 (2013) 12–18. doi:[10.1016/j.advwatres.2013.03.009](https://doi.org/10.1016/j.advwatres.2013.03.009).
615 URL <https://linkinghub.elsevier.com/retrieve/pii/S0309170813000493>
- 616 [57] A. AghaKouchak, **A baseline probabilistic drought forecasting framework using standardized soil moisture index: application**
617 **to the 2012 United States drought**, Hydrology and Earth System Sciences 18 (7) (2014) 2485–2492. doi:[10.5194/hess-18-2485-2014](https://doi.org/10.5194/hess-18-2485-2014).
618 URL <https://hess.copernicus.org/articles/18/2485/2014/>
- 619 [58] R. D. Garreaud, J. P. Boisier, R. Rondanelli, A. Montecinos, H. H. Sepúlveda, D. Veloso-Aguila, **The Central Chile**
620 **Mega Drought (2010–2018): A climate dynamics perspective**, International Journal of Climatology 40 (1) (2020) 421–439.
621 doi:[10.1002/joc.6219](https://doi.org/10.1002/joc.6219).
622 URL <https://rmets.onlinelibrary.wiley.com/doi/10.1002/joc.6219>
- 623 [59] M. Abramowitz, I. A. Stegun, Handbook of mathematical functions with formulas, graphs, and mathematical tables,
624 Vol. 55, US Government printing office, 1968.
- 625 [60] D. S. Wilks, Empirical distributions and exploratory data analysis, Statistical Methods in the Atmospheric Sciences 100
626 (2011).
- 627 [61] Y. Zhao, D. Feng, L. Yu, X. Wang, Y. Chen, Y. Bai, H. J. Hernández, M. Galleguillos, C. Estades, G. S. Biging, J. D.
628 Radke, P. Gong, **Detailed dynamic land cover mapping of Chile: Accuracy improvement by integrating multi-temporal**
629 **data**, Remote Sensing of Environment 183 (2016) 170–185. doi:[10.1016/j.rse.2016.05.016](https://doi.org/10.1016/j.rse.2016.05.016).
630 URL <https://linkinghub.elsevier.com/retrieve/pii/S0034425716302188>
- 631 [62] P. K. Sen, **Estimates of the Regression Coefficient Based on Kendall's Tau**, Journal of the American Statistical Association
632 63 (324) (1968) 1379–1389. doi:[10.1080/01621459.1968.10480934](https://doi.org/10.1080/01621459.1968.10480934).
633 URL <http://www.tandfonline.com/doi/abs/10.1080/01621459.1968.10480934>
- 634 [63] M. Kendall, Rank correlation methods (4th ed, 2d impression). Griffin, 1975.
- 635 [64] R. Tibshirani, J. Bien, J. Friedman, T. Hastie, N. Simon, J. Taylor, R. J. Tibshirani, **Strong rules for discarding predictors**
636 **in lasso-type problems** (Nov. 2010).
637 URL <http://arxiv.org/abs/1011.2234>
- 638 [65] A. E. Hoerl, R. W. Kennard, **Ridge Regression: Biased Estimation for Nonorthogonal Problems**, Technometrics 12 (1)
639 (1970) 55–67. doi:[10.1080/00401706.1970.10488634](https://doi.org/10.1080/00401706.1970.10488634).
640 URL <http://www.tandfonline.com/doi/abs/10.1080/00401706.1970.10488634>
- 641 [66] T. K. Ho, Random decision forests, in: Proceedings of 3rd international conference on document analysis and recognition,
642 Vol. 1, IEEE, 1995, pp. 278–282.
- 643 [67] S. M. Vicente-Serrano, D. Peña-Angulo, S. Beguería, F. Domínguez-Castro, M. Tomás-Burguera, I. Noguera, L. Gimeno-
644 Sotelo, A. El Kenawy, **Global drought trends and future projections**, Philosophical Transactions of the Royal Society A:
645 Mathematical, Physical and Engineering Sciences 380 (2238) (2022) 20210285. doi:[10.1098/rsta.2021.0285](https://doi.org/10.1098/rsta.2021.0285).
646 URL <https://royalsocietypublishing.org/doi/10.1098/rsta.2021.0285>
- 647 [68] S. M. Vicente-Serrano, D. G. Miralles, F. Domínguez-Castro, C. Azorin-Molina, A. El Kenawy, T. R. McVicar, M. Tomás-
648 Burguera, S. Beguería, M. Maneta, M. Peña-Gallardo, **Global Assessment of the Standardized Evapotranspiration Deficit**
649 **Index (SEDI) for Drought Analysis and Monitoring**, Journal of Climate 31 (14) (2018) 5371–5393. doi:[10.1175/JCLI-D-17-0775.1](https://doi.org/10.1175/JCLI-D-17-0775.1).
650 URL <https://journals.ametsoc.org/doi/10.1175/JCLI-D-17-0775.1>
- 651 [69] M. Meroni, F. Rembold, D. Fasbender, A. Vrieling, **Evaluation of the Standardized Precipitation Index as an early**
652 **predictor of seasonal vegetation production anomalies in the Sahel**, Remote Sensing Letters 8 (4) (2017) 301–310. doi:
653 [10.1080/2150704X.2016.1264020](https://doi.org/10.1080/2150704X.2016.1264020).
654 URL <https://www.tandfonline.com/doi/full/10.1080/2150704X.2016.1264020>
- 655 [70] A. Miranda, A. D. Syphard, M. Berdugo, J. Carrasco, S. Gómez-González, J. F. Ovalle, C. A. Delpiano, S. Vargas, F. A.
656 Squeo, M. D. Miranda, C. Dobbs, R. Mentler, A. Lara, R. Garreaud, **Widespread synchronous decline of Mediterranean-**
657 **type forest driven by accelerated aridity**, Nature Plants 9 (11) (2023) 1810–1817. doi:[10.1038/s41477-023-01541-7](https://doi.org/10.1038/s41477-023-01541-7).
658 URL <https://www.nature.com/articles/s41477-023-01541-7>
- 659 [71] F. Kogan, W. Guo, W. Yang, **Near 40-year drought trend during 1981–2019 earth warming and food security**, Geomatics,
660 Natural Hazards and Risk 11 (1) (2020) 469–490. doi:[10.1080/19475705.2020.1730452](https://doi.org/10.1080/19475705.2020.1730452).
661 URL <https://www.tandfonline.com/doi/full/10.1080/19475705.2020.1730452>
- 662 [72] V. Potopová, P. Stepánek, M. Mozný, L. Türkott, J. Soukup, Performance of the standarised precipitation evapotranspi-
663 ration index at various lags for agricultural drought risk assessment in the {C}zech {R}epublic, Agricultural and Forest
664 Meteorology 202 (2015) 26–38.
- 665 [73] M. Dai, S. Huang, Q. Huang, G. Leng, Y. Guo, L. Wang, W. Fang, P. Li, X. Zheng, **Assessing agricultural drought risk**
666 **and its dynamic evolution characteristics**, Agricultural Water Management 231 (2020) 106003. doi:[10.1016/j.agwat.2020.106003](https://doi.org/10.1016/j.agwat.2020.106003).
667 URL <https://linkinghub.elsevier.com/retrieve/pii/S0378377419316531>

- 671 [74] M. Taucare, B. Viguier, R. Figueroa, L. Daniele, **The alarming state of Central Chile's groundwater resources: A paradigmatic case of a lasting overexploitation**, Science of The Total Environment 906 (2024) 167723. doi:[10.1016/j.scitotenv.2023.167723](https://doi.org/10.1016/j.scitotenv.2023.167723).
672 URL <https://linkinghub.elsevier.com/retrieve/pii/S0048969723063507>
- 673 [75] C. Senf, A. Buras, C. S. Zang, A. Rammig, R. Seidl, **Excess forest mortality is consistently linked to drought across Europe**, Nature Communications 11 (1) (2020) 6200. doi:[10.1038/s41467-020-19924-1](https://doi.org/10.1038/s41467-020-19924-1).
674 URL <https://www.nature.com/articles/s41467-020-19924-1>
- 675 [76] A. Fathi-Taperasht, H. Shafizadeh-Moghadam, M. Minaei, T. Xu, **Influence of drought duration and severity on drought recovery period for different land cover types: evaluation using MODIS-based indices**, Ecological Indicators 141 (2022) 109146. doi:[10.1016/j.ecolind.2022.109146](https://doi.org/10.1016/j.ecolind.2022.109146).
676 URL <https://linkinghub.elsevier.com/retrieve/pii/S1470160X22006185>
- 677 [77] C. Wu, L. Zhong, P. J.-F. Yeh, Z. Gong, W. Lv, B. Chen, J. Zhou, J. Li, S. Wang, **An evaluation framework for quantifying vegetation loss and recovery in response to meteorological drought based on SPEI and NDVI**, Science of The Total Environment 906 (2024) 167632. doi:[10.1016/j.scitotenv.2023.167632](https://doi.org/10.1016/j.scitotenv.2023.167632).
678 URL <https://linkinghub.elsevier.com/retrieve/pii/S0048969723062599>
- 679 [78] C. Xiao, S. Zaehle, H. Yang, J.-P. Wigneron, C. Schmullius, A. Bastos, **Land cover and management effects on ecosystem resistance to drought stress**, Earth System Dynamics 14 (6) (2023) 1211–1237. doi:[10.5194/esd-14-1211-2023](https://doi.org/10.5194/esd-14-1211-2023).
680 URL <https://esd.copernicus.org/articles/14/1211/2023/>
- 681 [79] A. Venegas-González, A. A. Muñoz, S. Carpintero-Gibson, A. González-Reyes, I. Schneider, T. Gipolou-Zuñiga, I. Aguilera-Betti, F. A. Roig, **Sclerophyllous Forest Tree Growth Under the Influence of a Historic Megadrought in the Mediterranean Ecoregion of Chile**, Ecosystems 26 (2) (2023) 344–361. doi:[10.1007/s10021-022-00760-x](https://doi.org/10.1007/s10021-022-00760-x).
682 URL <https://link.springer.com/10.1007/s10021-022-00760-x>
- 683 [80] V. Humphrey, A. Berg, P. Ciais, P. Gentile, M. Jung, M. Reichstein, S. I. Seneviratne, C. Frankenberg, **Soil moisture-atmosphere feedback dominates land carbon uptake variability**, Nature 592 (7852) (2021) 65–69. doi:[10.1038/s41586-021-03325-5](https://doi.org/10.1038/s41586-021-03325-5).
684 URL <https://www.nature.com/articles/s41586-021-03325-5>
- 685 [81] W. Zhang, F. Wei, S. Horion, R. Fensholt, M. Forkel, M. Brandt, **Global quantification of the bidirectional dependency between soil moisture and vegetation productivity**, Agricultural and Forest Meteorology 313 (2022) 108735. doi:[10.1016/j.agrformet.2021.108735](https://doi.org/10.1016/j.agrformet.2021.108735).
686 URL <https://linkinghub.elsevier.com/retrieve/pii/S0168192321004214>
- 687 [82] L. Samaniego, S. Thober, R. Kumar, N. Wanders, O. Rakovec, M. Pan, M. Zink, J. Sheffield, E. F. Wood, A. Marx, **Anthropogenic warming exacerbates European soil moisture droughts**, Nature Climate Change 8 (5) (2018) 421–426. doi:[10.1038/s41558-018-0138-5](https://doi.org/10.1038/s41558-018-0138-5).
688 URL <https://www.nature.com/articles/s41558-018-0138-5>
- 689 [83] S. Chatterjee, A. R. Desai, J. Zhu, P. A. Townsend, J. Huang, **Soil moisture as an essential component for delineating and forecasting agricultural rather than meteorological drought**, Remote Sensing of Environment 269 (2022) 112833. doi:[10.1016/j.rse.2021.112833](https://doi.org/10.1016/j.rse.2021.112833).
690 URL <https://linkinghub.elsevier.com/retrieve/pii/S0034425721005538>